THERMAL PROTECTION OF HIGH TEMPERATURE POLYMER-MATERIAL-CARBON FIBER COMPOSITES

A Thesis

by

JUSTIN EARL O'NEAL

Submitted to the Office of Graduate Studies of
Texas A&M University
in partial fulfillment of the requirements for the degree of

MASTER OF SCIENCE

December 2005

Major Subject: Mechanical Engineering

THERMAL PROTECTION OF HIGH TEMPERATURE POLYMER-MATERIAL-CARBON FIBER COMPOSITES

A Thesis

by

JUSTIN EARL O'NEAL

Submitted to the Office of Graduate Studies of
Texas A&M University
in partial fulfillment of the requirements for the degree of

MASTER OF SCIENCE

Approved by:

Chair of Committee:	Roger Morgan
Committee Members:	Sai Lau
	Michael Bevan
Head of Department:	Dennis O'Neal

December 2005

Major Subject: Mechanical Engineering

ABSTRACT

Thermal Protection of High Temperature

Polymer-Material-Carbon Fiber Composites. (December 2005)

Justin Earl O'Neal, B.S., Texas A&M University

Chair of Advisory Committee: Dr. Roger Morgan

Two evaporative-cooling materials were studied which are (i) salt hydrates and (ii) polyacrylic acid for the purpose showing proof of concept of being able to put evaporative-cooling materials into a composite with the Air Force polyimide AFR-PEPA-N. The salt hydrates were observed to absorb water and then evaporate water, but due to having a collapsible lattice, made them incapable of reabsorbing water. Polyacrylic acid was mixed into an epoxy sheet at polacrylic acid weight percentages of 5, 10, 12.5. For each weight percentage there was a hydrated epoxy specimen and a dry epoxy specimen. All specimens were individually shot with a hot air stream (temperature approximately 130^{0}C). Temperature readings were taken for each sheet. The hydrated specimen exhibited greater evaporative cooling over its dry counterpart. 12.5 wt% was shown to have the best evaporative cooling mechanism. Experiments were repeated to show that the polyacrylic could reabsorb water. This study illustrates proof of concept utilizing polyacrylic acid as an evaporative cooling material.

ACKNOWLEDGMENTS

I would like to thank my committee chair, Dr. Roger Morgan, for his financial support and guidance. I would like to thank Dr. Sai Lau and Dr. Michael Bevan for being on my committee.

I would like to thank Eric Strickland for being my right-hand man for this experiment. I would like to also thank Yuntao Li and Michael Shatruk for their guidance.

I would like to thank Dr. Dennis O'Neal for helping me with the understanding of the heat transfer laws involved with my experiment.

I would like to thank Greg Payette for his exchange of knowledge regarding the physical laws involved in this experiment.

I would like to thank Ysidoro Ramirez for allowing me to use the Data Acquisition System; otherwise, this experiment would be impossible.

I would like to thank Dr. Thomas Lalk for his guidance on uncertainty.

TABLE OF CONTENTS

TABLE OF CONTENTS (CONT.)

LIST OF FIGURES

LIST OF FIGURES (CONT.)

LIST OF TABLES

CHAPTER I

INTRODUCTION

Focus of Research

This research is conducted for the United States Air Force and is funded by the State of Texas under the Advanced Technology Program. Research is conducted in the Polymer Technology Center at Texas A&M University, College Station, Texas. Dr. Roger Morgan served as the head of the project, and Dr. Sai Lau and Dr. Michael Bevan served on the research committee.

Motivation

Modern aerospace applications require high-performance materials such as high-temperature polymer matrix composites for the exterior of stealth aircraft. High performance materials will also be used for cryogenic fuel containment structures for future space vehicles. Two types of high temperature polymer matrix composites are (i) cross-linked bismaleimide, BMI, thermoset, and (ii) thermoplastic polyimide. [1]

This thesis follows the style of Energy Conversion & Management.

The Air Force has an interest in polyimides that exhibit good mechanical properties at high temperatures, hydrolytic resistant, and form complex shape structures. These polyimides must be able to be produced by low viscosity resin transfer molding with the product being lightweight. Stresses produced by processing must be minimal, to limit microcracking formation during application. The composite damage growth mechanisms must be known for both the microscopic and macroscopic dimesional levels. [2]

The Air Force initially considered AFR 700B (Figure 1) for their polyimide as use for stealth aircraft. Unfortunately AFR 700B had norbornene crosslinkable end caps, which could not withstand hygrothermal exposure. At 160^0C for 1000 hours in a hygrothermal pressure bomb environment, AFR 700B was found to lose about 30% of its strength with a reduction in its glass transition temperature (T_g). [2]

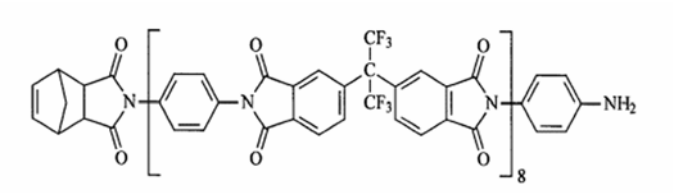

Fig. 1. AFR700B chemical structure

In studies, phenylethynyl end capped based polyimides, such as PETI-5 (Figure 2) showed a much greater resistance to hydrolytic degradation. Researchers considered to putting phenylethynyl end caps to AFR 700B to increase hydrolytic resistance, the resultant product being AFR-PEPA-N (Figure 3). [2]

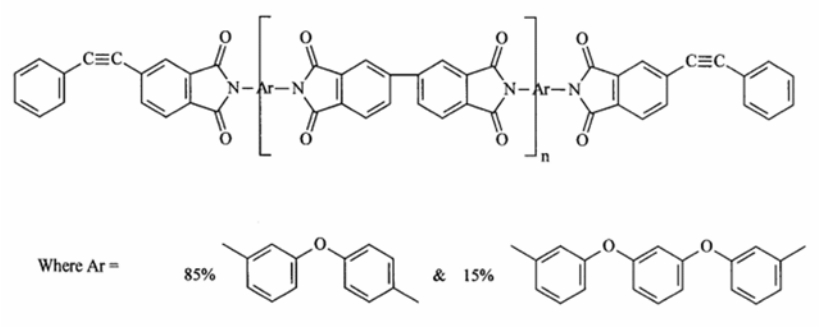

Fig. 2. PETI-5 chemical structure

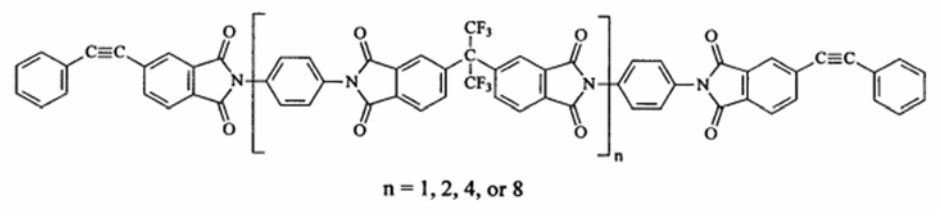

Fig. 3. AFR-PEPA-N imide oligomer chemical structure

AFR-PEPA-N was tested at the Air Force Research Laboratories. Under hygrothermal exposure, AFR-PEPA-N experienced only a 3-5% decrease in dry T_g as opposed to AFR 700B which experienced a 20% decrease in dry T_g under similar conditions. Other positive characteristics of AFR-PEPA-N are (i) high ductility, (ii) able to be processed by transfer resin molding, and (iii) superior mechanical properties over AFR 700B. [2]

AFR-PEPA-N has the potential to be used on stealth aircraft and space vehicles, both of which will have to endure extreme service environment conditions. AFR-PEPA-N has already been used on the trailing edges of the stealth B-2 Bomber. [2]

In order for AFR-PEPA-N to function to its highest potential, it needs to be formed into composite mixed with evaporative-cooling materials. The evaporative-cooling materials that this study will consider are (i) salt hydrates and (ii) polyacrylic acid for proof o of concept only. In theory, when a vehicle travels at high Mach speeds of 2-3, evaporative-cooing materials absorb heat due to an increase of temperature, they will experience a dehydration of their own water molecules, which will cool the surface. These evaporative dehydration mechanisms cause cooling of the inorganic composite. This phenomenon causes a stealth vehicle (such as an aircraft) to reduce its exterior temperature and thermal signature. With a reduction in thermal signature, there will be a lesser possibility that a stealth aircraft will get shot down by a heat-seaking missile. A thermal signature can be detected if there is a deviation greater than 1^0C between the aircraft and its surroundings [3]. The Soviet Union used moisture bearing fibers (30% weight) of polyamidobenzimidazole "in their intercontinental ballistic missile rocket motor casings to limit thermal-induced damage from laser threats" [3].

A previous study has shown the accelerated cooling of an evaporative model compared to a thermal conductivity model (Figure 4). The evaporative model represents a composite with 15% weight moisture, and the thermal conductivity model represents "thermal conduction through a 1 cm thick composite to an interior 23^0C cooling pipe sink". [3]

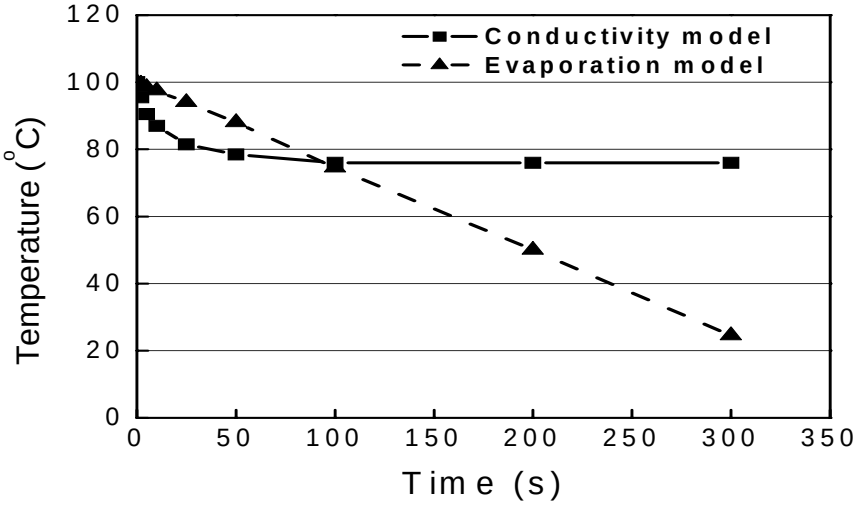

Fig. 4. Comparison of composite surface cooling by thermal conduction versus moisture evaporation

Background on Evaporative Cooling

Biological evaporative cooling exists in the sweat glands under human skin (Figure 5). Sweat glands (Figure 6) are simple coils of colloidal epithelium located in the hypodermis or deep dermis. This biological mechanism can transport 0.5-10 liters/day of 99% pure water to the surface. [3]

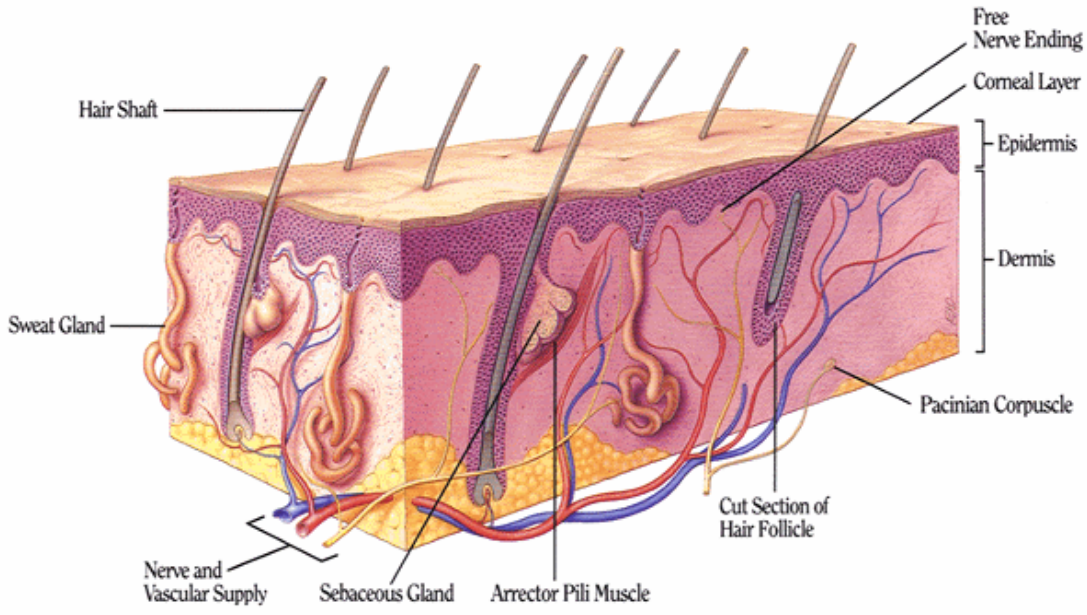

Fig. 5. Structure of the skin

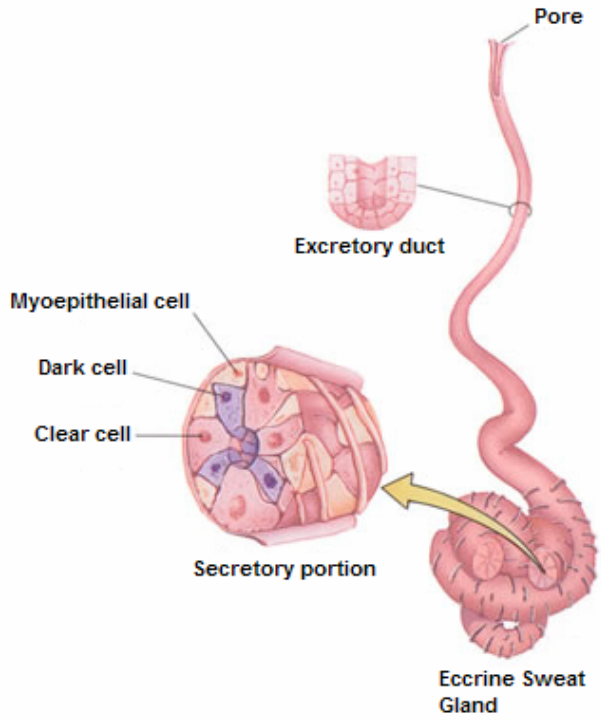

Fig. 6. The eccrine sweat gland

Animals use evaporative cooling as a secondary means of lowering body temperature in hot climates; the primary means is thermoregulation such as getting under shaded areas. Animals have upper lethal body temperature (different from the ambient temperature) where there fundamental chemistry starts failing. Vertebrates, except birds which are more tolerant, have an upper lethal temperature of 45^0C, while insects have an upper lethal temperature of 48^0C. [4]

The internal temperature of an animal is usually different than ambient temperature. Bees withstanding ambient temperatures of 52^0C can withhold body temperatures at 48^0C for thirty minutes and then die. Evaporative cooling is more efficient at a lower relative humidity than a high relative humidity. At 45^0C and 90% relative humidity a cockroach had a internal temperature of 45^0C; at 45^0C in dry air a cockroach's internal temperature will fall to 39^0C in a few minutes. The rate of evaporation can be increased with increased surface area and increased velocity of the ambient air over the surface. Heat loss is a function of the mass of water evaporated at *2.4kJ/g* [4]. Conduction is the main mechanism of heat transfer in evaporative cooling according to one source [5]. Convection is the heat transfer mechanism according to another source where convective heat transfer coefficient increase as evaporation increases transfers large amounts of energy [6].

Some species of insects have unique ways of evaporative cooling when dealing with high ambient temperatures. The Glosssina morsitans feeds on blood and while feeding will have abundant supply of water for evaporative cooling; it can lower its body temperature

by 2^0C in 45^0C dry air. When the Perga dorsalis reaches a body temperature of 37^0C, it will discreet liquid from its anus and spread on its body; it is able to keep its body temperature below 42^0C at an ambient temperature of 48^0C. [4]

The Cicada Okanagodes Gracilis can lose 25% of their body mass through evaporative cooling and still survive. It replenishes its water supply by constant feeding which prevents osmoregulatory problems. Osmoregulatory problems are common in small animals due to high surface area to volume ratio, small size, and limited water supply. Higher temperatures increase the rate of evaporative cooling. Cicadas have a light green or tan coloration which serves as cryptic coloration and enhanced reflectivity. Lighter-colored specimens heat more slowly in hot environments than darker-colored specimens; lighter-colored specimens reflect more radiation than darker-colored specimens. [7]

Due to the 1973 oil crisis and the following rise of oil prices, the American population realized their dependency on the oil-producing countries. After which, increasing interests in reducing energy costs at all levels of society became a general goal in engineering circles [8]. Evaporative cooling is used as a low-cost alternative to air conditioning in homes in dry climates. Evaporative cooling can also be used to cool industrial or commercial buildings. This process uses a heat exchanger to produce cool moist air to lower the temperature of dry air which is used to cool the environment. The cool moist air is removed to ambient, thus there is no adding moisture to the dry air. This process requires no energy except to operate the fan and water pump, which would result

in a high coefficient of performance [9]. Some evaporative cooling models utilize the pressure supply line to eliminate the required use of a water pump [10].

The process of evaporation is the governing step for cooling towers, evaporative condensers, evaporative fluid coolers, evaporative air coolers and dehumidifying coils. These devices usually have the water sprayed, sprinkled or poured over packing as opposed to releasing absorbed water as in the epoxy resin [11]. “Evaporative cooling has also found applications in such areas as the drying of gelcast ceramics, shrinkage of foods due to moisture removal, cryogenic freezing of ammonia in supersonic flow, thermal bending in precision machine tools, cooling of high power density electronic devices, and numerous other passive, low energy consumption processes [12].”

Early History of Polyimides

1908 marked the first year of polyimide synthesis, although it was during the 1950s when high molecular weight polymers were first being manufactured [13].

In December of 1955 at DuPont’s Film Department at the Experimental Station in Wilmington, Delaware, A. L. Endrey led a team to research “convertible polymers”, an approach to aromatic polyimides. The result ended in the polyimide Polymer E, which due to its aromatic structure would be more thermally stable than polyethylene terephalate [14].

In March of 1956, Andy Endrey had a research assignment to seek an aromatic polyimide prepared by a soluble intermediate polymeric precursor. After a month, he determined that dimethylformamide (DMF) could be used as synthesis of poly(amic-acid). Later, he produced the first poly(amic-acid) film and was able to achieve both thermal and chemical conversion to polyimide film [14].

Dupont produced the first patents for polyimides in 1959 and 1960 in Europe and Australia. Dupont released the first paper of polyimides at the Philadelphia American Chemical Society in April 1964. In October 1965, the first full-scale production of polyimide film began, designated as Kapton; shortly therafter, Dupont released Vespel (polyimide molding) and Pyre-ML (polyimide wire insulation). The National Aeronautics and Space Administration (NASA) developed many polyimides including bis-maleimide composites, colorless polyimides, the LARC polyimide series, and poly(imide/etherketone) copolymers. Japanese research utilized phenolic solvents for the preparation of polyimides. Ube Industries developed Upilex series of polyimides, which are produced from biphenyl dianhydride (BPDA). Occidental Chemical Company were able to produce polyimides with excellent hydrolytic durability in addition to having a variety of mechanical and electrical properties. Mitsui-Toatsu, NASA, and DuPont have produced melt-processible polyimides [14].

Background on Salt Hydrates

The salt hydrates that are planned to be tested are sodium sulfate decahydrate ($Na_2SO_4 \cdot 10H_2O$) and copper sulfate pentahydrate ($CuSO_4 \cdot 5H_2O$).

When these salt hydrates absorb heat due to an increase of temperature, they will experience a dehydration of their water molecules. This evaporative dehydration causes cooling of the inorganic hydrate-resin composite.

Initially weaker bonded water molecules are removed at lower temperatures and then stronger bonded molecules are removed at higher temperatures. For $CuSO_4 \cdot 5H_2O$, the four water molecules are in an octahedral coordination group around the copper atom. The fifth water molecule is held by hydroxyl bonds to the SO_4^{2-} ion, which will remove at a temperature above 200^0C (Table 1) [15].

Table 1 The decomposition stages of copper sulfate pentahydrate

Stage	T_{range} (K)	Decomposition
1	327-380	$CuSO_4 \cdot 5H_2O \rightarrow CuSO_4 \cdot 3H_2O + 2H_2O$
2	380-421	$CuSO_4 \cdot 3H_2O \rightarrow CuSO_4 \cdot H_2O + 2H_2O$
3	505-553	$CuSO_4 \cdot H_2O \rightarrow CuSO_4 + H_2O$

For $Na_2SO_4 \cdot 10H_2O$, eight water molecules are in an octahedral coordination group, and the last two are involved in hydroxyl (hydrogen) bonding [16]. Sodium sulfate

decahydrate degrades in a similar manner as copper sulfate pentahydrate; its water sequence with relevant temperature ranges could not be found in literature.

Background on Polyacrylic Acid

In addition to hydrates another product: polyacrylic acid (PAA) is considered as a water-absorbing agent. Polyacrylic acid can absorb 30 times its weight in water, or about 30mL of water per gram [17]. COO^- is a hydrophilic functional group (Figure 7) [18]. Modern baby diapers contain polyacrylic acid because it is hydrophilic [17]. Water molecules attached to polyacrylic acid by hydrogen bonds with a bond energy of approximately 5 kcal/mole [19]. Polyacrylic acid is a cross-linked polymer [20]. Higher molecular weights of polyacrylic acid have a potential for higher water adsorption due to an increase in moisture absorbing segments [21], but counteracting water is the polymer having hydrogen bonding with its own hydrocarbon chains [22]. As molar mass of polyacrylic acid increases its hydrocarbon chains fold into each other [22]. The amount of water adsorption of polyacrylic acid will decrease with increasing pH, because increasing the pH will reduce the number of hydrogen donor groups (OH_2^+) [21]. Water attaches to polyacrylic acid by both hydrogen bonding and attaches to the carboxyl groups; the carboxyl groups act as both a proton donor and acceptor [21]. The presence of calcium will increase the adsorption of polyacrylic acid [21]. Polymers have the ability to preserve the water that they absorb [23]. Polyacrylic acid changes its size, form, and effective charge as a function of its concentration [24].

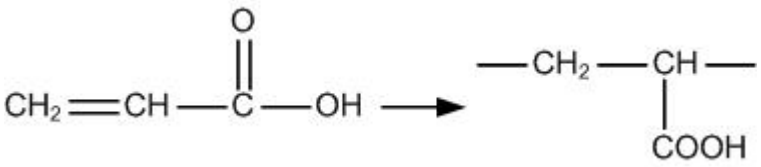

Fig. 7. Polyacrylic acid structure

To have a perspective on the thermal degradation of polyacrylic acid, the thermal degradation of polymethylacrylic acid (PMAA) (Figure 8) is considered. When polymethylacrylic acid is heated, it goes through cyclodehydration where the acid releases water to form six membered anhydride structures. Following first order kinetics, 21 kcal/mole is the activation for cyclodehydration in a temperature range of 180^0C-250^0C. Confirmed by IR spectra, cyclodehydration is complete at 250^0C. The formed anhydride groups are very stable will not decompose until some temperature above 300^0C. [25]

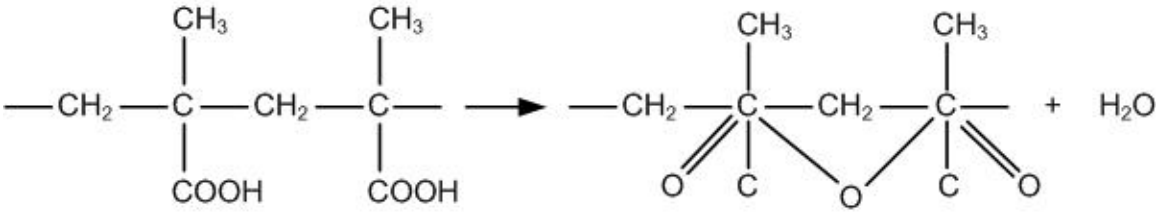

Fig. 8. Polymethylacrylic acid cyclodehydration

Polymethylacrylic acid has an activation of 40kcal/mole for its decomposition in a temperature range 370^0C-430^0C. Confirmed by IR spectra, polymethylacrylic acid

releases carbon dioxide around 400^0C. At higher temperatures, polymethylacrylic acid further decomposes by liberating carbon monoxide and hydrocarbons (Figure 9). [25]

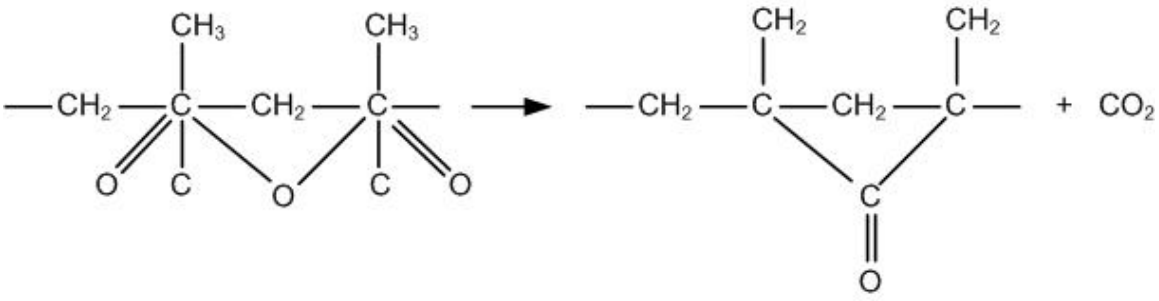

Fig. 9. Polymethylacrylic acid decomposition

Some sources say that PAA does go through cyclodehydration at different temperatures. One scientist used IR spectra to show that carbon dioxide was the main product of pyrolysis above 150^0C (decarboxylation) [25]. Differential thermal analysis' curve has shown endothermic maxima at 260^0C and 290^0C. Calculated values for the activation energy of decarboxylation of PAA range from 17-27 kcal/mole (Figure 10). [25]

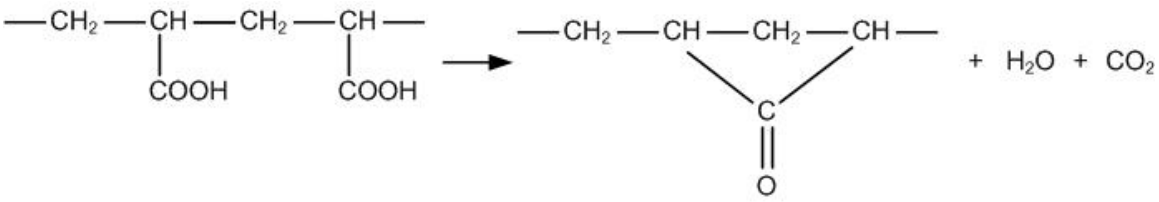

Fig. 10. Polyacrylic acid decarboxylation

The decarboxylation is a complex mechanism unlike the first-order kinetics of polymethylacrylic acid. Decarboxylation has a faster rate at a low pH versus a high pH.

Further degradation beyond 300^0C produces hydrogen (H_2), carbon monoxide (CO) and traces of hydrocarbon compounds such as acetylene, ethylene, and propane. This process is a multi-step degradation with each step having its own activation energy. This mechanism favors high pH levels at high temperatures. [26]

A lightly cross-linked version of polyacrylic acid – polycarbophil has been used for vaginosis and as a spermicide (Figure 11). [27]

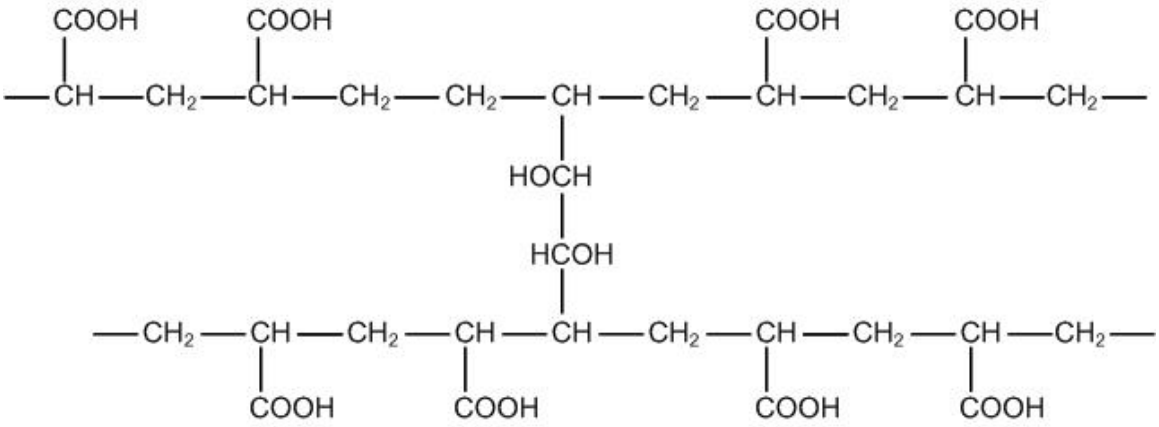

Fig. 11. Polycarbophil

This research project is concerned with an evaporative cooling mechanism to be used for stealth vehicles.

CHAPTER II

EXPERIMENTAL

Hydrates' Test

Crystals of both sodium sulfate decahydrate ($Na_2SO_4 \cdot 10H_2O$) and copper sulfate pentahydrate ($CuSO_4 \cdot 5H_2O$) were provided by Sigma Aldrich.

Crystals of sodium sulfate decahydrate are stored in an environment of 100% humidity. This environment is created by placing crystals of sodium sulfate decahydrate on a piece of cloth that is put on top of 250 mL beaker that is half-filled with water. This apparatus is stored in an enclosed volume for several days. This apparatus prevents the sodium sulfate decahydrate from evaporating off its own hydrates prematurely. This environment compels the crystals to absorb water molecules to their full potential. This process is repeated for crystals of copper sulfate pentahydrate.

Completely hydrated crystals are removed from the apparatus and are weighed and put into a Digital Scanning Calorimetry (DSC) machine. The DSC starts heating the crystals at 25^0C and is heated at 10^0C/min until the machine reaches its predetermined temperature (usually around 300^0C for this experiment). As each set of hydrates evaporates water off of the crystals a peak is produced on its Heat Flow vs. Temperature DSC curve. When the run is complete a curve with peaks representing evaporation should be produced.

Polyacrylic Acid

Crystals of Polyacrylic Acid (Figure 12) were provided by Sigma Aldrich. Polyacrylic acid is hydrated and run in a DSC in the same manner as the salt hydrates.

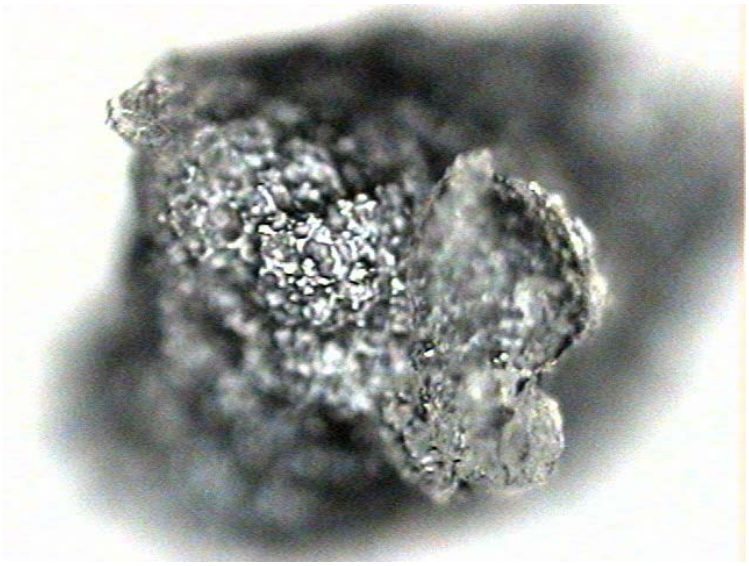

Fig. 12. Optical microscope photo of a hydrated polyacrylic acid crystal

Epoxy Sheets with Polyacrylic Acid

Particles of Polyacrylic Acid (PAA) are weighed in several aluminum pans. These pans containing PAA are put into a vacuum oven with a vacuum at 80^0C overnight to remove moisture. They are removed from the oven and then reweighed.

DER 332 bisphenol-A-diglycidyl ether epoxy (DGEBA) (Figure 13) was provided by Dow and diethylene triamine (DETA) (Figure 14) was provided by Sigma Aldrich. DGEBA is poured and weighed in a beaker and is heated to 60^0C for twenty minutes to melt any crystals that are present [28]. The DGEBA is removed from the oven and cooled down to room temperature. The DETA is poured into the DGEBA at eleven parts per hundred by weight [28]. The weighed polyacrylic acid is slowly added to the mixture while it is being stirred. After which, this mixture is poured in between two vertical Teflon plates. Rubber tubing is put between the Teflon to form the bottom half of the mold.

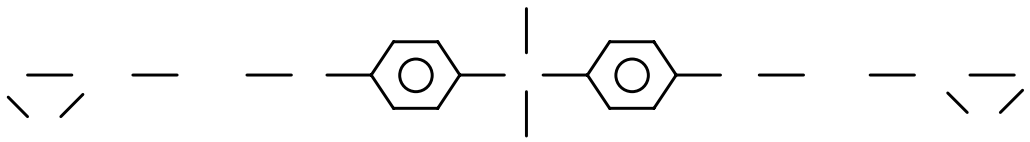

Fig. 13. Bisphenol-a-diglycidyl ether epoxy (DGEBA)

Fig. 14. Diethylene triamine (DETA)

The Teflon plates with the mixture and rubber tubing between them are put into an oven at 110^0C for two days at normal pressure. The mixture slowly cures to an epoxy sheet. After the second day, the plates are removed from the oven and allowed to cool to room

temperature. The formed epoxy sheet is removed from the plates by using a scraper. The epoxy sheet is cut into two halves by visual approximation.

One half (humid half) is put into a 100% humid environment for several days to absorb moisture. This humid environment is created by putting a 250 mL beaker filled with water in an enclosed environment with the epoxy sample (Figure 15).

Fig. 15. Humid chamber

The other half (dry half) of the epoxy sheet is put into a vacuum oven (Figure 16) with a vacuum at 80^0C for two days. The sheet is then put into a vacuum-pulled dessicator until it is tested.

Fig. 16. Vacuum oven

There will be a humid half and dry half for the following polyacrylic acid to epoxy system weight percentages: 5, 10, and 12.5.

Air Flow Test Setup

Both halves have the same test procedure. Thermocouples are attached to a sample with epoxy. Thermocouples are attached to the front surface, back surface, and side surface. Electrical tape is used to cover the thermocouple on the front surface to prevent measurements of air temperature; in other words, to obtain exclusively the temperature of the epoxy sheet. Electrical tape is also put on the back-surface thermocouple. For testing, each sample is held in place by metal grips.

Air is supplied from an air source and runs through plastic tubing (3/8 in. diameter). The plastic tubing runs into a flow meter (Figure 17). Plastic tubing leaves the flow meter and is connected to a coil of copper tubing. The flow meter used in Figure 17 is the smaller one to the left of the big one. Hose clamps are used for all of the plastic tubing connections. Thermolyne heating tape is woven around the copper tubing (Figure 18) to supply a heat source for the air flow. The heat flow of the heating tape is regulated by a temperature controller. Copper tubing is used because of its high heat conductivity. At the end of the copper tubing is a thermocouple to read the air's temperature which is connected with electrical tape. The copper tubing's outlet is used for the heated air flow.

Fig. 17. Flowmeter

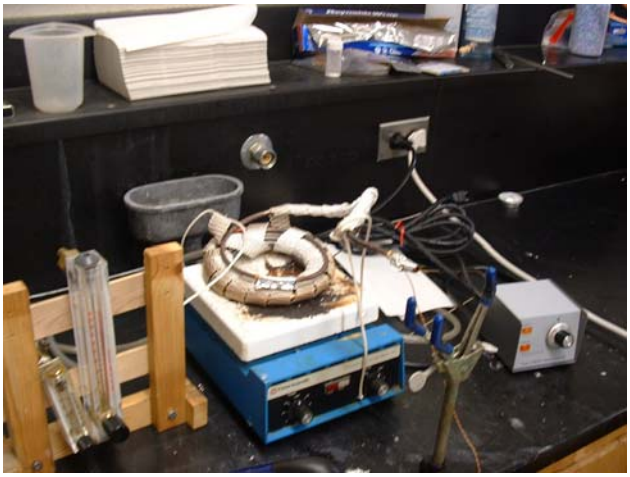

Fig. 18. Test apparatus

Air Flow Test Execution

All the thermocouples are connected into Texas Instrument's Data Acquisition System (Figure 19). To start, the Data Acquisition System is set to run to start collecting temperature readings for all four thermocouples (one for the air and three on the epoxy specimen). Thermocouple readings are made by a Data Acquisition System for each thermocouple for every second of the experiment. The air is turned on and set to 1.5 SCFM, which is monitored by the flow meter. The temperature controller is set to HIGH. While the air is traveling in the copper tubing, it is heated by the heating tape. The air is allowed to heat for 500 seconds to allow the air to reach a constant maximum temperature.

After 500 seconds has elapsed, an epoxy sheet is put into place and supported with metal grips (Figure 20). The copper tubing's outlet is aimed at the center of the epoxy sheet.

The distance between the outlet and the epoxy sheet is set at 2 inches. The three thermocouples on the epoxy sheet show a rise in temperature. When the experiment has run for additional fifteen minutes (900 seconds) after the original 500 seconds for a total of 1400 seconds, the air is shut down and the temperature controller is shut down and unplugged.

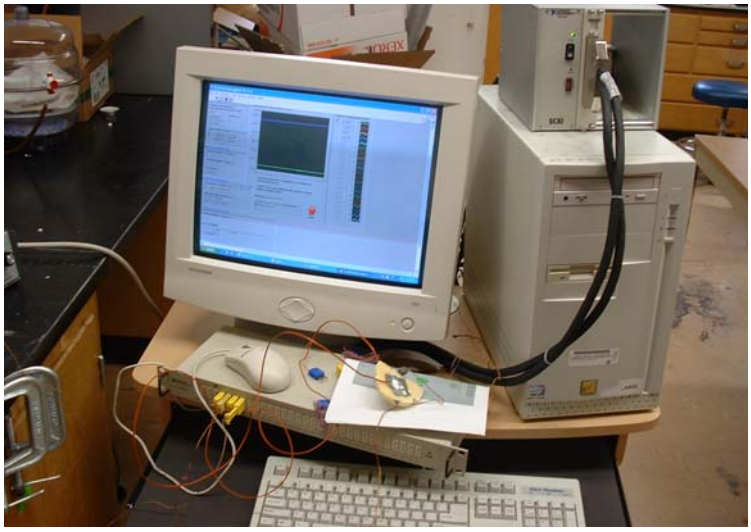

Fig. 19. Data acquisition system

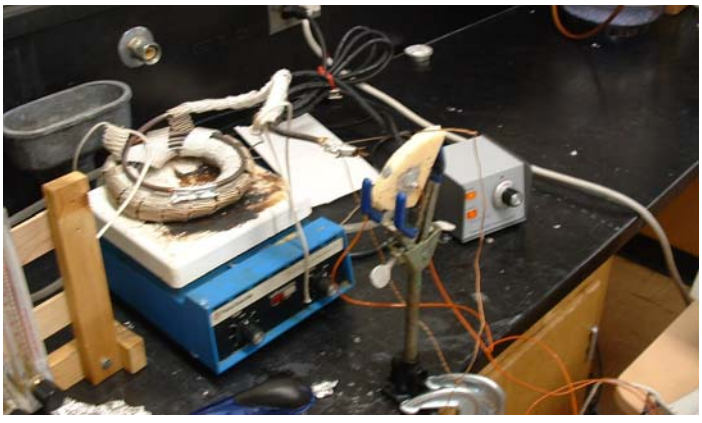

Fig. 20. Test apparatus with specimen

A total of six specimens were tested, both a dry and humid specimen for each of the following polyacrylic acid to epoxy system weight percentages: 5, 10, and 12.5. Temperature was examined as both a function of time and PAA concentration.

CHAPTER III

RESULTS AND DISCUSSION

Salt Hydrates

Figures 21 & 22 display the DSC readings of the first samples of both sodium sulfate decahydrate and copper sulfate pentahydrate. The first hydrated sample of sodium sulfate decahydrate weighed 10.59mg, and the first hydrated sample of copper sulfate pentahydrate weighed 7.51mg.

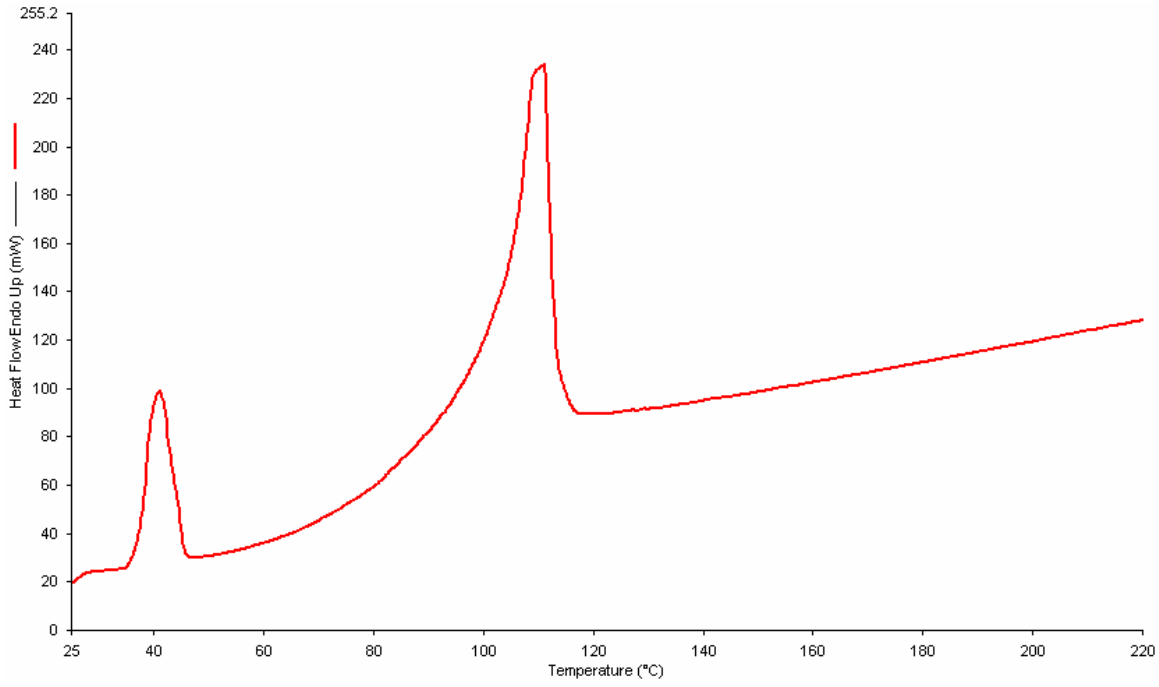

Fig. 21. Differential scanning calorimetry of sodium sulfate

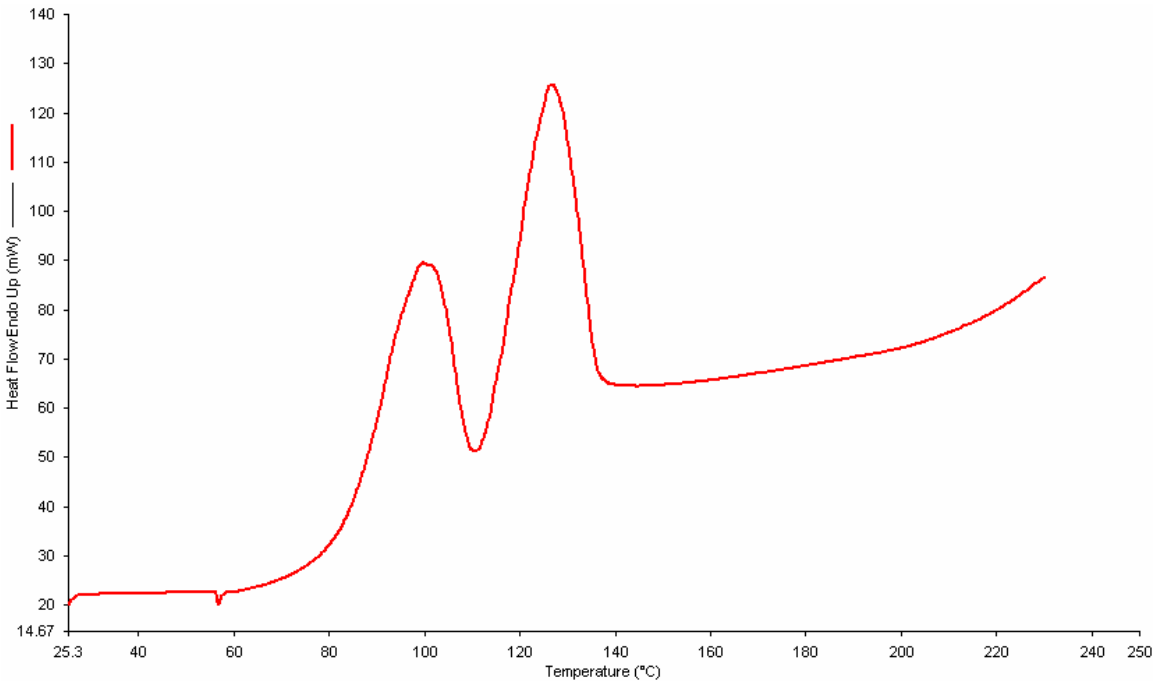

Fig. 22. Differential scanning calorimetry of copper sulfate

The computer calculates the area under the peak which is the amount of heat loss due to the H_2O evaporation of each set of hydrates. Using 2260 J/g (get reference) as the heat of evaporation for water and the heat loss of evaporation for each set of hydrates, the mass of water evaporated is calculated. This mass is converted into millimoles to calculate the number of moles lost due to water evaporation. Tables 2 & 3 show the heat absorbed and the water evaporated for both of the hydrates.

Table 2 Dehydration of the sodium sulfate

	Temperature (^{0}C)	Heat mJ	H_2O Mass (mg)	H_2O Millimoles
1st Peak	41	2164	0.957	0.053
2nd Peak	111	9121	4.036	0.224

Table 3 Dehydration of the copper sulfate

	Temperature (^{0}C)	Heat mJ	H_2O Mass (mg)	H_2O Millimoles
1st Peak	99	3930	1.739	0.097
2nd Peak	126	5081	2.248	0.125

Lack of Reusability of the Hydrates

After the samples were dehydrated by their DSC run, they were returned to the 100% humid environment to be hydrated again. After which, the samples were again weighed and put through the DSC apparatus. Similar DSC results were not repeatable; the original H2O evaporation peaks were absent. This showed that the hydrates were incapable of being hydrated after complete evaporation. After the crystals lost their water molecules, their crystal lattice collapses thus making them incapable of being hydrated again.

These salt hydrates only proved a concept of using evaporative-cooling materials as a one-time use for aircraft. Because the crystal lattice collapses after evaporation, any

similar product would be a onetime use for the cooling of such aircraft. For similar products to have long term impact on cooling stealth aircraft, they would be required to repaint the aircraft after every use; otherwise, thermal degradation will continue as if there were no materials cooling the surface at all. This required repainting of the cooling surfaces would be uneconomical considering extensive labor and product costs.

One source mentions that there exists hydrates that do not have a collapsible lattice [15]. A literature search for hydrates without a collapsible lattice was not successful.

Polyacrylic Acid

Because of the hydrates lack of reusability, another product: polyacrylic acid (PAA) is considered as a substitute. Unlike the salt hydrates, polyacrylic acid does not have a fragile crystal lattice. The DSC for the Polyacrylic Acid was measured on a different machine than the DSC for the hydrates (Figure 23). The hump diagram representing the evaporation of water is estimated at 769 mJ or 0.34 mg of water. The drastic increase of heat following the hump represents the point where the polyacrylic acid expands beyond the capacity of the test pan at which point DSC measurements becomes an impossibility.

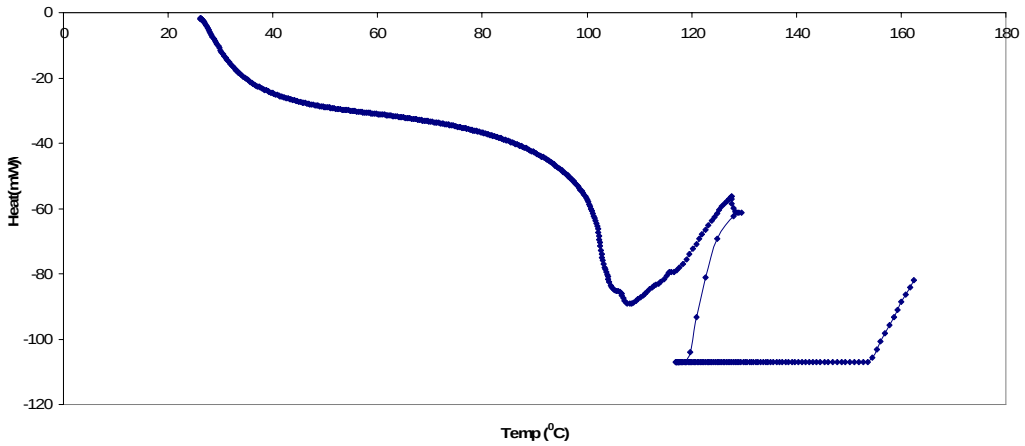

Fig. 23. Differential scanning calorimetry of polyacrylic acid

Air Flow Test

For each specimen, the actual amount of absorbed water can not be easily determined. However a relative amount of absorbed water can be easily measured. Table 4 shows the weight of each specimen before their treatment (either humid chamber or vacuum oven) and after their treatment. The difference represents either the amount of water absorbed or removed after their individual treatment.

Table 4 Water gain/loss for each specimen

	before treatment (g)		after treatment (g)	water gain/loss (g)	water gain/loss (%)
5 wt %	dry	28.6224	28.5666	-0.0558	-0.1950
1st run	humid	23.8697	24.4713	0.6016	2.5204
5 wt %	dry	29.0757	29.0067	-0.069	-0.2373
2nd run	humid	24.3281	25.1951	0.867	3.5638
10 wt %	dry	27.049	26.845	-0.204	-0.7542
1st run	humid	26.853	27.874	1.021	3.8022
10 wt %	dry	27.9749	28.987	1.0121	3.6179
2nd run	humid	28.919	29.5029	0.5839	2.0191
12.5 wt %	dry	27.6522	27.4521	-0.2001	-0.7236
1st run	humid	31.2753	32.405	1.1297	3.6121
12.5 wt %	dry	28.9051	28.2554	-0.6497	-2.2477
2nd run	humid	31.6817	32.6706	0.9889	3.1214

Each of the following graphs (Figures 24-29) represents a comparison of a humid and dry specimen using a specific polyacrylic acid concentration. The x axis is time (seconds) and the y axis is temperature (^{0}C). Each graph contains eight sets of data points; one for the thermocouple for the air for both specimens, and one for each of the three thermocouples on both specimens. This experiment is mainly focused on the temperature difference of the front surface for both specimens. The temperature rise at 500 seconds on the specimen thermocouples represents the point at which the specimen is put into place of the air flow.

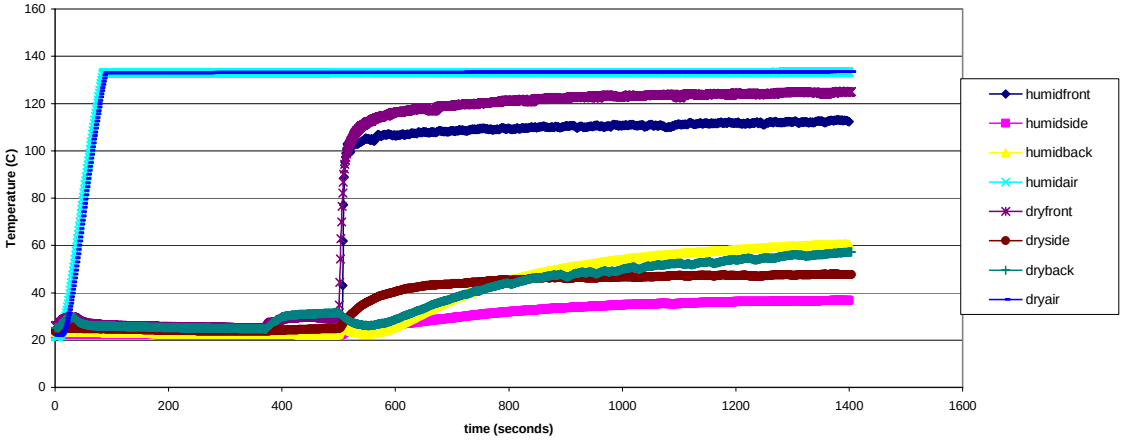

Fig. 24. Air flow test for 5 weight percent polyacrylic acid (1st run)

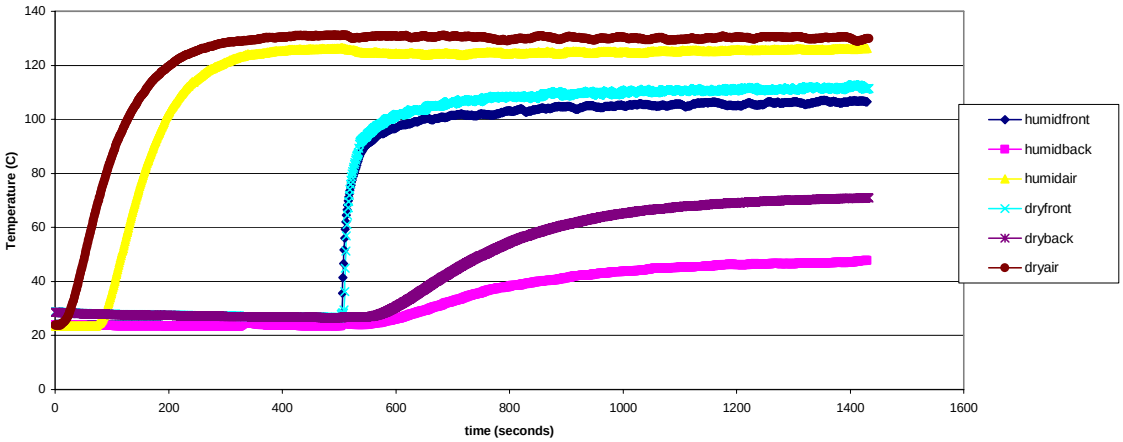

Fig. 25. Air flow test for 5 weight percent polyacrylic acid (2nd run)

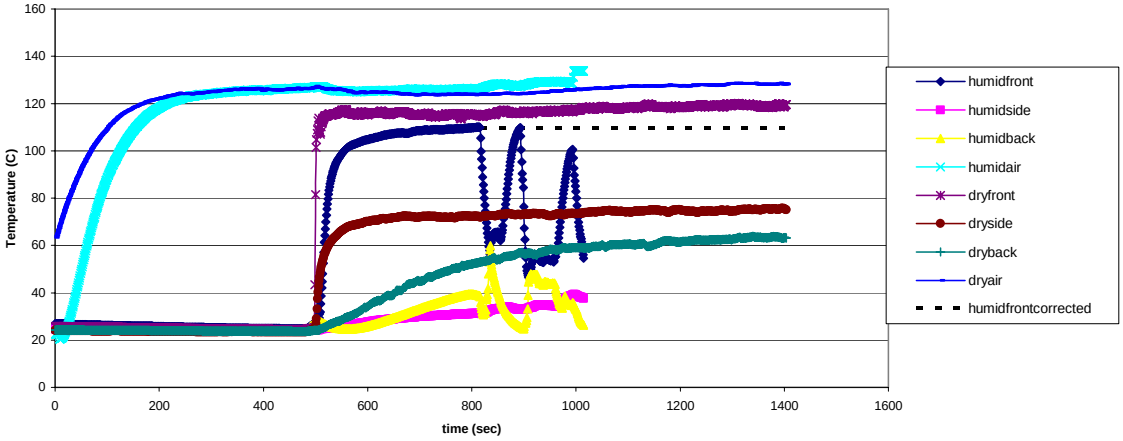

Fig. 26. Air flow test for 10 weight percent polyacrylic acid (1st run)

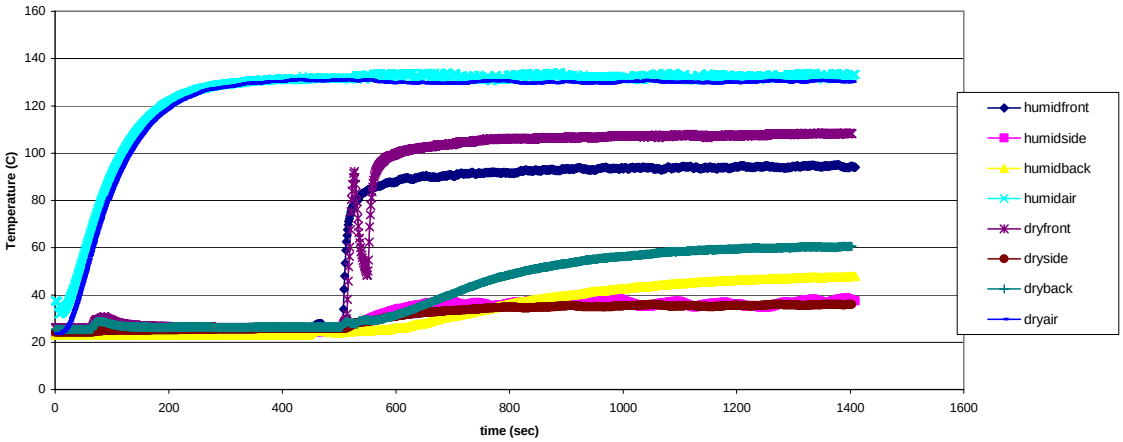

Fig. 27. Air flow test for 10 weight percent polyacrylic acid (2nd run)

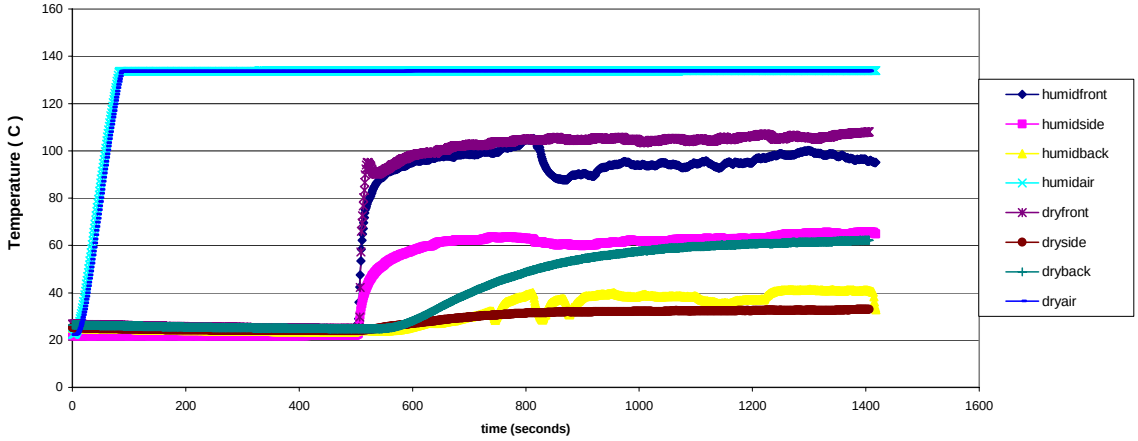

Fig. 28. Air flow test for 12.5 weight percent polyacrylic acid (1st run)

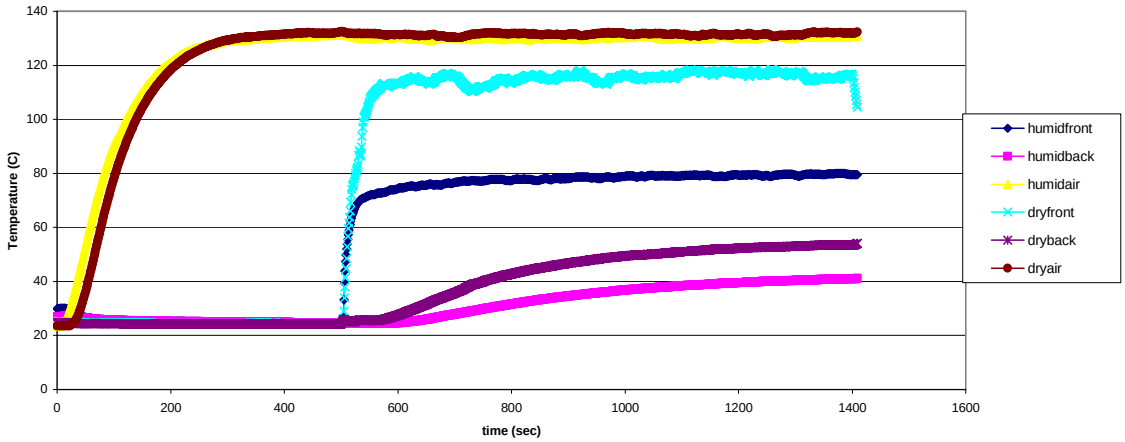

Fig. 29. Air flow test for 12.5 weight percent polyacrylic acid (2nd run)

For figure 26, there was a problem with the thermocouples coming off of the specimen, when this happened the thermocouples were put back on the specimen and quickly fell off again. However from the graph, the beginning of the asymptote can be seen before

the thermocouples fell off, a dotted line represents where the asymptote would have been had the thermocouples not fallen off the specimen.

Each of the graphs show that the asymptote for the humid specimen is significantly lower than the asymptote for its dry counterpart, although there may be quick temperature rise for the humid specimen before it lowers to an asymptotic temperature.

The percent difference (D) between the data points of the humid specimen and the dry specimen are calculated with the following formula:

$$D = \frac{x_{humidave} - x_{dryave}}{x_{dryave}} * 100\% \quad (1)$$

where $x_{humidave}$ is the average temperature of the humid specimen as it asymptotes, and x_{dryave} is the average temperature of the dry specimen as it asymptotes. Table 5 shows percent difference for each specimen comparison; the negative sign represents that there was a decrease in temperature due to the evaporative cooling.

Table 5 Percent difference between humid and dry specimens

	Average (T)		Percent Difference
5 wt % 1st run	dry	123.9256	
	Humid	110.331	-10.970
5 wt % 2nd run	dry	118.8051	
	Humid	108.9681	-8.280
10 wt % 1st run	dry	105.4391	
	Humid	95.88103	-9.065
10 wt % 2nd run	dry	110.7754	
	Humid	105.6261	-4.648
12.5 wt % 1st run	dry	107.4837	
	Humid	93.91717	-12.622
12.5 wt % 2nd run	dry	116.2765	
	Humid	79.14843	-31.931

Although for both runs, the five percent specimens had a better percent difference than the ten percent specimens, the average temperature for the ten percent specimens was lower than the five percent specimens. The 12.5% specimens showed the best percent difference.

Uncertainty

The degree of uncertainty for any experiment should be looked at when considering the results. Mainly, the accuracy uncertainty is the uncertainty of the thermocouples used, which the thermocouples are accurate within 1^0C.

Discussion

Because the degree of accuracy uncertainty does not compare with the percent difference (Table 5), in other words, the percent difference outweighs the uncertainty, evaporative cooling is shown to take place.

When comparing between graphs (i.e. 10 and 12.5 weight percent) both the dry and humid asymptotes for a higher polyacrylic acid concentration are lower than both the dry and humid asymptotes for the lower polyacrylic acid concentration. This shows that not all the water is removed in a dry specimen and there is some evaporative cooling taking place in the dry specimens. Higher polyacrylic acid concentration specimens are more likely to have more water in them than lower polyacrylic acid concentration specimens.

Completely Dry Specimen

An assumed completely dry specimen can have its heat transfer represented with a finite difference model. The heat transfer of the epoxy specimen involves the following: (1) the initial heat convection from the jet stream onto the facing surface of the epoxy specimen, (2) the heat conduction through the epoxy specimen, and (3) the heat convection off the back side of the specimen to the surrounding room temperature. Figure 30 shows a diagram of the epoxy specimen's heat transfer. The heat is traveling from left to right. Each Temperature Mark (T#) represents a temperature node for doing a finite difference model. Figure 30 is not set to scale, it has been elongated height wise

to show temperature nodes. The distance between nodes (Δx) is the distance between the front side and the back side of the epoxy specimen (1cm) divided by six. h_{air} is the convection coefficient of the jet stream air and h_{room} is the free convection coefficient of the surrounding room temperature air.

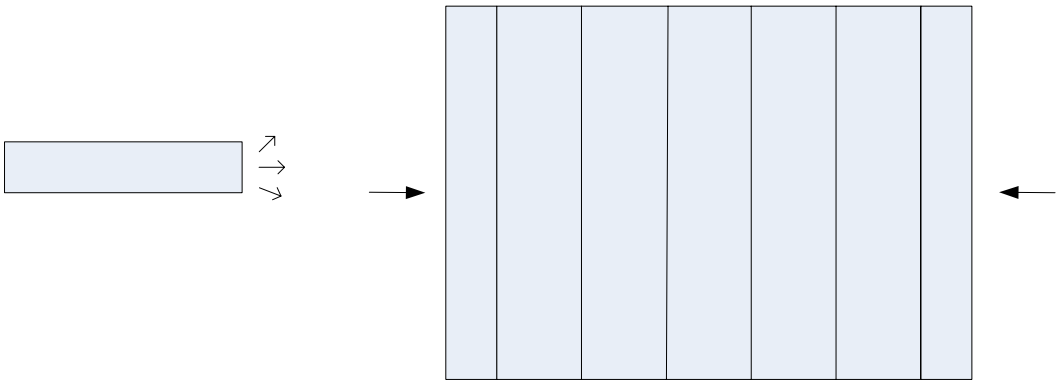

Fig. 30. Finite difference model of a completely dry specimen

To set up a spreadsheet model of the change of temperature (Celsius) at each node as a function time (Δt per time increment is one second) involves series of equations. First, the following equation is a finite-difference model to represent the convection at the front surface and the conduction just past the surface:

$$T_0^{p+1} = 2Fo(T_1^p + BiT_{air}) + (1 - 2Fo - 2BiFo)T_0^P \quad (2)$$

where (p) represents at specific point in time (seconds),

$$Fo = \frac{\alpha \Delta t}{(\Delta x)^2} \quad \text{, and} \quad (3)$$

$$Bi = \frac{hair\, \Delta x}{k}. \quad (4)$$

α is the diffusivity which is calculated by

$$\alpha = \frac{k}{\rho c_p}. \tag{5}$$

The conductivity (k) and the specific heat (c_p) of the epoxy specimen must either be known or estimated by known values of similar materials. The density (ρ) can be calculated by dividing its mass by its volume. [29]

Second, the conduction through the epoxy specimen can be modeled by

$$T_m^{p+1} = T_m^p (1 - 2Fo) + Fo(T_{m+1}^p + T_{m-1}^p). \tag{6}$$

as a function of time at each node. [29]

Finally, the convection at the node at the backside of the epoxy specimen can be calculated as a function similar to the convection at the front side of the node by

$$T_6^{p+1} = 2Fo(T_5^p + BiT_{room}) + (1 - 2Fo - 2BiFo)T_6^P. \tag{7}$$

The Bi number is calculated in terms of h_{room}. [29]

The convection coefficients both h_{air} and h_{room} are calculated by a systematic means; one for the impinging jet and the other for the standard room temperature air. To calculate h_{air}, one first must calculate the Reynold's number of the air flow by

$$\mathrm{Re} = \frac{\rho V D_h}{\mu} \tag{8}$$

where ρ is the density at the average temperature between the jet stream air and the temperature of the front surface ($T_{ave1}=(T_{air}+T_0)/2$, T_{air} is about 130^0C, P is about 1 atm).

T_0 will change with time until it asymptotes and will have minimal change with time. V is the velocity which can be calculated by dividing the volumetric flow (1.5 ft^3/min) by the area of the outlet with a 3/8in diameter is 0.110 in^2. D_h is the hydraulic diameter of the outlet which is four times the area divided by the perimeter (D_h=4A/P). μ is the viscosity of T_{ave1}. Both viscosity and density are found either from tables or computer program. With the Reynold's number (Re), diameter of the outlet (3/8in, D), the distance between the outlet and the epoxy (2in, H), estimated radius of the epoxy specimen if the corner's were rounded off (r), the Prandtl number of the air (Pr), and the conductivity (k) of the air know, the convection coefficient (h_{air}) of the jet stream can be estimated. The Prandtl number and the conductivity are found by tables or computer program. With the following equations:

$$F1 = 2\,\mathrm{Re}^{1/2}(1 + 0.005\,\mathrm{Re}^{0.55})^{1/2}, \tag{9}$$

$$G = \frac{D}{r}\frac{1 - 1.1D/r}{1 + 0.1(H/D - 6)D/r}, \tag{10}$$

$$Nu = G * F1 * \mathrm{Pr}^{0.42}, \text{ and} \tag{11}$$

$$h_{air} = \frac{Nu\,k}{D_h}, \tag{12}$$

h_{air} can be approximated. [29]

The free convection coefficient h_{room} is a function of the node T_6 which will change with time; therefore, h_{room} will change with time. An average temperature (T_{ave2}) between T_{air} and T_6 would be used to determine the property values of the air. T_6 will change with time until it asymptotes and thus the degree of change will be minimal. The following

property values of air would be based on T_{ave2}: Prandtl number (Pr), conductivity (k), kinematic viscosity (ν), and the beta term (β) which is $1/T_{ave2}$. With the length of the back side of the epoxy specimen (L, 2in), the acceleration of gravity (g), and the following equations:

$$Gr_L = \frac{g\beta(T_6 - T_{air})L^3}{\upsilon^2}, \tag{13}$$

$$Ra_L = \Pr^* Gr_L, \tag{14}$$

$$Nu_L = \left\{0.825 + \frac{0.387 Ra_L^{1/6}}{\left[1 + (0.492/\Pr)^{9/16}\right]^{8/27}}\right\}^2, \text{ and} \tag{15}$$

$$h_{room} = \frac{Nu_L k}{L}, \tag{16}$$

the free convection coefficient (h_{room}) of the backside can be estimated. [29]

Water Diffusion

When considering a hydrated epoxy specimen, as the front surface is heated with the impinging air, an evaporative cooling mechanism will take place to lower the surface temperature. Water will evaporate off of the surface. Water from the interior of the epoxy specimen specifically in the polyacrylic acid will diffuse to the front surface where it will continue to supplement the evaporation process (Figure 31). The mathematics of the water diffusion are beyond the scope of this experiment. The water diffusion mechanism will be dependent upon the temperature gradient and how densely packed the epoxy molecules are. Water has a tendency to move to a higher temperature, the higher

temperature at the surface than compared to the temperature at the location of the individual water molecules will cause the water molecules to diffuse to the surface. A more densely packed epoxy specimen will hinder the rate of diffusion as compared to a less densely packed epoxy specimen.

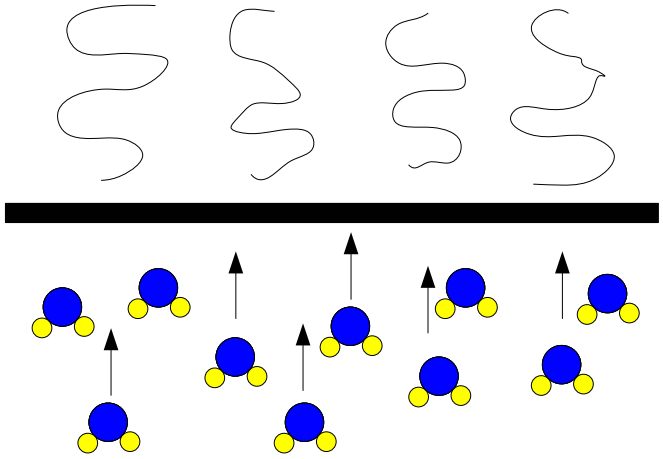

Fig. 31. Water diffusion to the evaporating surface

Evaporating Surface

For a hydrated specimen when the evaporation at the surface is taking place, it will cause some suction at the surface [30]. Figure 32 shows the heat balance at the evaporating surface.

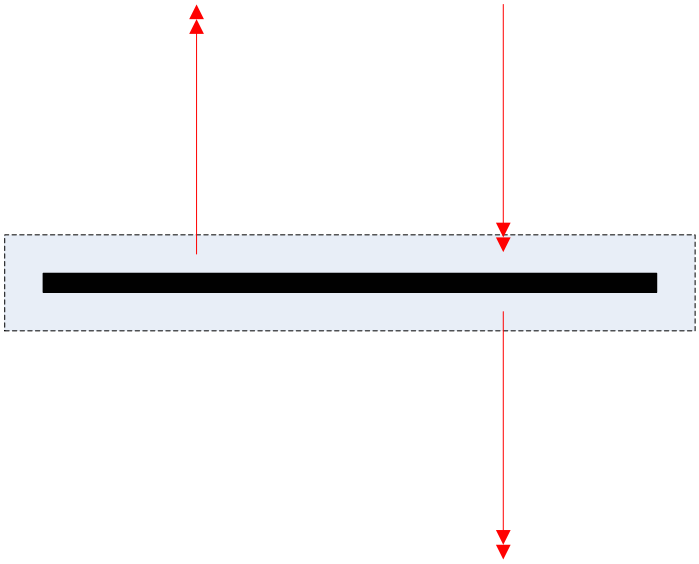

Fig. 32. Heat balance at the evaporating surface

The heat balance is represented by

$$q_{cond} + q_{evap} = q_{conv} . \tag{17}$$

The heat of conduction (q_{cond}) is represented by

$$q_{cond} = -k \frac{T_{back} - T_s}{L} \tag{18}$$

where k is the thermal conductivity of the epoxy specimen, T_s is the front surface surface temperature, T_{back} is the back surface temperature, and L is the length of the epoxy specimen. [29]

The heat of convection (q_{conv}) is represented by

$$q_{conv} = h_{air} A(T_s - T_{air}) \tag{19}$$

where A is the front surface area. [29]

The heat of evaporation (q_{evap}) is represented by

$$q_{evap} = \dot{m} h_{fg} \tag{20}$$

where h_{fg} is enthalpy of evaporation of water which is found in a thermodynamics table and $\dot{m}$ is the evaporation rate of water. The evaporation rate of water is calculated by

$$\dot{m} = h_m A(\rho_s - \rho_{air}) \tag{21}$$

where h_m is the convective mass transfer coefficient, ρ_s is the vapor density at the surface, and ρ_{air} is the vapor density of the jet stream. The vapor densities are found from psychrometric chart which require relative humidity values for both the surface and the jet stream; the relative humidity values were not found for this experiment. [30]

To determine h_m, first the Reynold's number (eqn. 8) using air properties that based on an average temperature [T_{ave3}=(T_s+T_{air})/2] between the jet stream and the surface must be calculated and it should be a laminar flow. With room pressure (p) at 1 atm, the following unit-dependent can be solved to the find mass diffusivity (D_v) number:

$$D_v = \frac{1.46 * 10^{-4}}{p}\left(\frac{T_{ave3}^{2.5}}{T_{ave3} + 441}\right) \tag{22}$$

where D_v is in ft^2/h, p in atm, and T_{ave} is in ^{0}R. With the density (ρ), viscosity (μ), length of the front surface (2in, L), mass diffusivity (D_v) and the Reynolds number known with the following system of equations with units adjusted for consistency:

$$Sc = \frac{\mu}{\rho D_v}, \tag{23}$$

$$Sh = 0.664\,\mathrm{Re}^{1/2}\,Sc^{1/3}, \text{ and} \tag{24}$$

$$h_m = \frac{S_h D_v}{L}, \tag{25}$$

the mass transfer coefficient (h_m) can be approximated. [30]

CHAPTER IV

CONCLUSION

Summary

The Air Force has an interest in polyimides that exhibit good mechanical properties at high temperatures, hydrolytic resistant, and form complex shape structures. Specifically, AFR-PEPA-N (Figure 3) will be used as a polyimide on stealth aircraft and space vehicles and has already been used on the trailing edges of the B-2 Bomber. [2]

In order for AFR-PEPA-N to function to its highest potential and rapidly minimize IR signatures from aerodynamic heating, it needs to be formed into a composite mixed with moisture evaporative-cooling materials. The evaporative-cooling materials that were studied to show proof of concept were both (i) salt hydrates and (ii) polyacrylic acid.

The salt hydrates were shown to have a collapsible lattice, where the lattice would collapse when the water molecules evaporated from the lattice. This phenomenon causes the salt hydrates to be incapable of reabsorbing water.

Polyacrylic acid does not have a collapsible lattice. When mixed into an epoxy sheet, a hydrated polyacrylic-acid-epoxy system is able to exhibit an evaporative cooling mechanism when confronted with hot temperatures. Higher concentrations of

polyacrylic-acid in the epoxy system will allow more absorption of water and thus better cooling than lower concentrations of polyacrylic-acid.

Recommendations

First, the hydrated epoxy sheets were shown to exhibit evaporation. However to quantitatively calculate the rate of evaporation requires the humidity values at both the front surface and the air stream (eqn. 21). This experiment, if repeated, could be improved by having the humidity measured at both the front surface and the air stream.

Finally, polyacrylic acid, even though used for both baby diapers and spermicide (Doan, Robinson), has shown a proof of concept of using evaporative-cooling materials in AFR-PEPA-N. This study shows that a greater concentration of hydrated polyacrylic acid in a composite system can cause more cooling than a lower concentration of polyacrylic acid. An evaporate-cooling material that is commercially manufactured into AFR-PEPA-N should use the highest weight percent may be possible. Because these experiments were repeated with the same material, this shows the possibility of reusability. With any evaporative cooling mechanism, cooling will be greater in a low humid environment than in a hot humid environment. However, because of the low thermal stability of polyacrylic acid, future development would involve more thermally stable, moisture absorbing polybenzimidazole fillers in AFR-PEPA-N.

REFERENCES

[1] Morgan R. J., Shin E. E., Lincoln J., Zhou J. Overview of polymer matrix composites performance and materials development for aerospace applications. SAMPE Journal 2001;37(2):102-107.

[2] Morgan R. J. Characterization of the structure-processing-performance relations phenylethynyl phthalic anyride crosslinked fluorinated polyimides (AFR-PEPA-N) and their carbon fiber composites, [Proposal], Dept. of Mechanical Engineering,Texas A&M University, College Station, Texas. 2003.

[3] Morgan R. J., Creasy T., Reddy J.N. Thermal protection/light weight materials development for future air force vehicles, [Proposal], Dept. of Mechanical Engineering, Texas A&M University, College Station, Texas. 2005.

[4] Prange H. D. Evaporative cooling in insects. Journal of Insect Physiology. 1996;42(5):493-499.

[5] Marzo M D., Tartarini P., Liao Y. Evaporative cooling due to a gently deposited droplet. International Journal of Heat and Mass Transfer 1993;36(17):4133-4139.

[6] Ghosal M.K., Tiwari G.N., Srivastava N.S.L. Modeling and experimental validation of a greenhouse with evaporative cooling by moving water film over external shade cloth. Energy and Buildings 2003;35:843-850.

[7] Sanborn A. F.,Heath J. E., Heath M. S. Thermoregulation and evaporative cooling in the cicada *okanagodes gracilis* (*homoptera: cicadidae*). Comp Biochem Physiol 1992;102A(4):751-757.

[8] Martinez F. J. R.,Gomez E. V., Martin H. R., Gutierrez J. M., Diez F. V. Comparitive study of two different evaporative systems: an indirect evaporative cooler. Energy and Buildings 2004;36:696-708.

[9] Riffat S.B., Zhu J. Mathematical model of indirect evaporative cooler using porous ceramic and heat pipe. Applied Thermal Engineering 2004;24:457-470.

[10] Al-Sulaiman F. Evaluation of the performance of local fibers in evaporative cooling. Energy Conversion and Management 2002;43:2267-2273.

[11] Halasz, B. A general mathematical model of evaporative cooling devices. Rev Gen Therm 1998;37:245-255.

[12] Hall C. A. III, Mackie C. Semi-analytic solutions for freezing induced by evaporative cooling. International Journal of Heat and Mass Transfer 2001;44:

1161-1170.

[13] Wilson, D., Stenzenberger H.D., Hergenrother P.M.. Polyimides. New York: Blackie & Sons; 1990.

[14] Ghosh, Malay K., K. L. Mittal K.L. Polyimides: Fundamentals and Applications. New York: Marcel Dekker; 1996.

[15] Olszak-Humienik M., Mozejko J. Eyring parameters of dehydration processes. Thermochimica Acta 2003;405:171-181.

[16] Ruben H. W., Templeton D. H., Rosenstein R. D., Olovsson I. Crystal structure and entropy of sodium sulfate decahydrate. [Paper] Dept. of Mechanical Engineering, Texas A&M University, College Station, Texas. 1960

[17] Doan, J. P. Self-cleaning surfaces – next revolution. [Class Paper] Dept. of Mechanical Engineering, Texas A&M University, College Station, Texas. 2005.

[18] Kandori K., Yamoto Y., Ishikawa T. Effects of vinyl series polymers on the dormation of hematite particles in a forced hydrolysis reaction. Journal of Colliod and Interface Science 2004;283:432-439.

[19] Saniger J. M., Hu H, Castano V. M. Kinetic studies of the dehydration process for polyacrylic acid-metal oxide compounds. Materials Letters.1992;15:113-117.

[20] Lee K. R., Teng M. Y., Lee H. H., Lai J. Y. Dehydration of ethanol/water mixtures by pervaporation with composite membranes of polyacrylic acid and plasma-treated polycarbonate. Journal of Membrane Science. 2000;164:13-23.

[21] Santhiya N., Nandini G., Subramanian S., Natarajan, K. A., Malghan S.G. Effect of polymer molecular weight on the absorption of polyacrylic acid at the alumina-water interface. Colloids and Surfaces A: Physicochemical and Engineering Aspects 1997;133:157-163.

[22] Misra D. N. Adsorption of polyacrylic acids and their sodium salts on hydroxyapatite: effect of relative molar mass. Journal of Colloid and Interface Science 1996;181:289-296.

[23] Ma C. J., Kasahara M., Tohno S. Application of polymeric water absorbent film to the study of drop size-resolved fog samples. Atmospheric Environment 2003;37:3749-3756.

[24] Porcar I., Codoner A., Gomez C. M., Abad C., Campos A. Interactions of quinine with polyacrylic and poly-l-glutamic acids in aqueous solutions. European Polymer Journal 2004;40:819-828.

[25] Kabanov V.P., Dubnitskaya V.A., Khar'kov S.N. Thermal properties of polyacrylic acid. All-Union Scientific Research Institute for Man-Made Fibers. 1974;April: 1848-1854.

[26] Lepine L., Gilbert R. Thermal degradation of polyacrylic acid in dilute aqueous solution. Polymer Degradation and Stability 2002;75:337-345.

[27] Robinson J. R., Bologna W. J. Vaginal and reproductive system treatments using a bioadhesive polymer. Journal of Controlled Release 1994;28: 87-94.

[28] Morgan, R. J. The effect of thermal history and strain rate on the mechanical properties of diethylenetriamine-cured-bisphenol-a-diglycidyl ether epoxies. Journal of Applied Polymer Science 23:2711-2717

[29] Incropera F. P., DeWitt D. P. Fundamentals of Heat and Mass Transfer. New York: John Wiley & Sons; 1996.

[30] ASHRAE Handbook. Atlanta, Georgia: American Society of Heating, Refrigerating and Air-Conditioning Engineers, Inc; 2005.

VITA

Name: Justin Earl O'Neal

Address: 1704 Springwood Ct., College Station, TX 77845

Email Address: justineo2002@yahoo.com

Education: M.S. Mechanical Engineering, Texas A&M University, 2005
B.S. Chemical Engineering, Texas A&M University, 2003

Work Experience: Texas A&M University, Dept. of Mechanical Engineering, Spring-Fall 2005, Spring-Summer 2004, Fall 2003

Lockheed Martin Aeronautics, Ft. Worth, TX. Fall 2004

Sandia National Laboratories, Albuquerque, NM, Summer 2003, Summer 2002, Summer 2001

Texas A&M University, Thermodynamics Research Center, Summer 2000